Molecular dynamic simulation study on co-aggregation between amyloid-β and Medin*

PAN Wenyan[1], CHENG Chuanyong[1], NIU Jingjing[1], YUAN Bing[2], YANG Kai[1], DONG Xuewei[1,3]

1.Center for Soft Condensed Matter Physics and Interdisciplinary Research & School of Physical Science and Technology, Soochow University, Suzhou 215006, China

2.Songshan Lake Materials Laboratory, Dongguan 523808, China

3.State Key Laboratory of Surface Physics, Fudan University, Shanghai 200433, China

Abstract

The aggregation of Medin is closely related to the arterial wall degeneration and cerebrovascular dysfunction. In patients with vascular dementia or Alzheimer's disease, the concentration of Medin in cerebral arterioles increases, and Medin is co-localized with vascular amyloid-β (Aβ) deposits. Previous study demonstrates that Medin interacts directly with Aβ, forming heterologous fibrils with Aβ and promoting Aβ aggregation. However, the basic mechanism of the co-aggregation between Medin and Aβ remains largely elusive. Here, we explore the interactions and conformational ensembles of $A\beta_{42}$/Medin trimers in different peptide environments (self-aggregation vs. co-aggregation) by performing all-atom replica exchange molecular dynamic simulation on $A\beta_{42}$/Medin homotrimers and $A\beta_{42}$-Medin heterotrimer with an accumulated simulation time of 72 μs. Our results reveal that $A\beta_{42}$ exhibits higher affinity with Medin, and $A\beta_{42}$ and Medin have similar molecular recognition sites in self-aggregation and co-aggregation. The N-terminus of $A\beta_{42}$ and the C-terminus of Medin play critical roles in $A\beta_{42}$-Medin cross-talk. More importantly, co-aggregation significantly changes the interaction strength, binding patterns and structural characteristics of $A\beta_{42}$ and Medin. Intermolecular interactions of $A\beta_{42}$ trimers are relatively weak among three trimers, and the binding sites are concentrated between N- and N-termini, between N- and C-termini, and between C- and C-termini of $A\beta_{42}$. In contrast, intermolecular interactions of Medin trimers are the strongest, and the binding sites are widely and uniformly distributed in Medin peptides. Intermolecular interactions of $A\beta_{42}$ in $A\beta_{42}$-Medin heterotrimer decrease compared with those of $A\beta_{42}$ trimers, only the binding of the hydrophobic core

---

* The paper is an English translated version of the original Chinese paper published in Acta Physica Sinica. Please cite the paper as: **PAN Wenyan, CHENG Chuanyong, NIU Jingjing, YUAN Bing, YANG Kai, DONG Xuewei, Molecular dynamic simulation study on co-aggregation between amyloid-β and Medin.** *Acta Phys. Sin.*, 2025, 74(15): 158701. doi: 10.7498/aps.74.20250616

regions (^{16}KLVFFA^{21}) is retained and other regions of $A\beta_{42}$ gain increase flexibility. Two-dimensional free energy landscapes reveal distinct conformational diversities between the homo- and heterotrimers, with the order of diversity being Medin/Aβ42-Medin trimers > $A\beta_{42}$ trimers. The R_g of $A\beta_{42}$ trimers is smaller than those of the other two trimers, implying that $A\beta_{42}$ trimers possess a more compact structure, whereas Medin/$A\beta_{42}$-Medin trimers exhibit a relatively loose conformation. The $A\beta_{42}$ trimers possess the highest β content whereas Medin trimers exhibit the lowest β probability. It is found that $A\beta_{42}$-Medin co-aggregation induces Medin to form more β-structures with longer lengths and fewer helices, while promoting $A\beta_{42}$ to form more helices and fewer β-structures. High β-propensity regions of Medin in heterotrimers shift towards the C-terminus of Medin, suggesting that Medin utilizes its C-terminal β region as a core motif to drive its co-aggregation with $A\beta_{42}$. These results elucidate the detailed influences of co-aggregation on the interactions and conformations of $A\beta_{42}$ and Medin. This work provides key insights into the molecular mechanism of $A\beta_{42}$-Medin co-aggregation and the pathological mechanisms of cross-linking between related diseases.

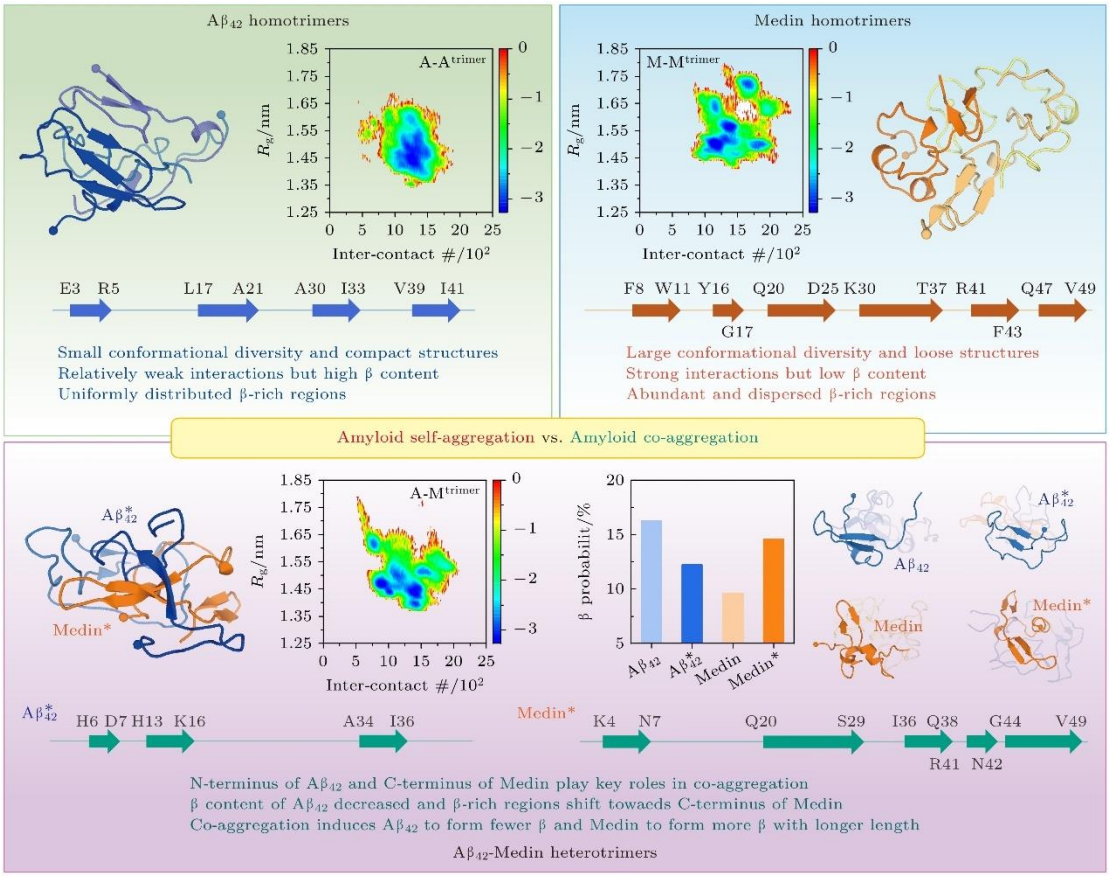

Keywords: peptide co-aggregation, amyloid-β, Medin, molecular dynamic simulations

PACS：87.15.nr, 87.14.ef, 87.10.Tf

doi: 10.7498/aps.74.20250616

cstr: 32037.14.aps.74.20250616

1. Introduction

Alzheimer disease (AD) is one of the most common neurodegenerative diseases affecting millions of people worldwide[1,2]. One of its pathological features is the deposition of amyloid fibrils produced by the misfolding and aggregation of amyloid-β protein (Aβ) in the brain. There are many subtypes of Aβ peptides, the most common of which are $A\beta_{40}$ and $A\beta_{42}$. Compared with $A\beta_{40}$, $A\beta_{42}$ has stronger aggregation ability and neurotoxicity[3–5]. In recent years, the role of Aβ in the pathogenesis of AD has been gradually revealed, especially in the mechanism of Aβ forming amyloid plaques and causing nerve cell damage[6,7]. Medin, as a common amyloid protein, widely exists in the vascular system and is closely related to aortic medial amyloidosis (AMA)[8–11]. Although specific amyloid lesions are usually caused by one type of amyloid protein, in actual cases[12,13], different types of amyloid proteins may coexist in the same tissue or organ[14–17]. This phenomenon of amyloid deposition may lead to multiple amyloidosis diseases, which not only increases the risk of complications, but also makes the disease more serious[18,19]. Studies have shown that Medin can directly interact with Aβ to promote Aβ aggregation and heterogenous fibril formation, and the cross-talk between Medin and Aβ may play a key role in the pathogenesis of AD and Vascular dementia (VaD)[20]. Therefore, it is of great significance to further study the interaction between $A\beta_{42}$ and Medin and its role in related amyloidosis, which is the focus of current research in related fields. By combining molecular dynamic (MD) simulations and various experimental methods, researchers have carried out a large number of studies on Medin and its related proteins, including the mechanism of Medin produced by MfgE8 cleavage, the three-dimensional structure of supramolecular assemblies formed by $Medin_{19\text{-}36}$-derived peptides, the structural and mechanistic differences between wild type Medin and its D25N mutant fibril formation, the conformational transition of Medin monomer and potential fibrillation mechanism, Medin folding and dimerization[21–26]. However, the microscopic mechanism of Medin and Aβ co-aggregation at the atomic level and the conformational transition of intrinsically disordered Medin and Aβ in aggregation are still not fully understood.

MD simulation is based on classical mechanics and statistical thermodynamics to describe the microstate evolution of a system. It is an important and powerful theoretical tool to study the dynamic behavior of biological macromolecules such as proteins and phospholipids at the atomic/molecular level. It is widely used to study protein-protein, protein-phospholipid interactions and various biological processes related to protein/cell membranes[27–30]. Due to the rapid aggregation of amyloid peptide and the dynamic variation of oligomer conformation, it is challenging to characterize the transient conformation of peptide oligomer by experimental means. MD simulation can provide an important supplement to experimental information, give the conformational characteristics of amyloid peptide oligomers at the

atomic scale of space-time resolution, and then reveal the microscopic mechanism of amyloid peptide assembly at the molecular level[31,32]. However, traditional MD simulations tend to fall into the local energy minimum state, which makes it difficult to sample the entire conformational space of complex protein systems in an acceptable simulation time[33]. Therefore, based on MD, a variety of computational simulation methods with enhanced sampling have been developed, including replica exchange molecular dynamic (REMD)[34], accelerated molecular dynamic (AMD)[35] and umbrella sampling[36]. The REMD simulation method was originally proposed by Sugita and Okamoto[34] in studies related to biomolecules. By combining MD simulations with Monte Carlo algorithms, REMD can easily overcome high energy barriers and fully sample the protein conformational space over a wider range, thus efficiently exploring the free energy landscape of protein aggregates[33]. REMD has been widely used to study the conformational distribution[37–39] of amyloid peptides and theirs fragments, the regulation of peptide conformation by mutation/post-translational modification[40,41], and the interaction[42–44] between peptides and small molecules/cell membranes/carbon nanotubes.

In this study, extensive all-atom REMD simulations were used to study the conformational ensembles and interaction details of homogeneous and heterogeneous $A\beta_{42}$ and Medin trimers. By analyzing the peptide-peptide interaction, the residue-residue contact number, the two-dimensional conformational free energy landscape, and the secondary structure, our results demonstrate in detail the significant effects of $A\beta_{42}$ – Medin co-aggregation on the interaction strength and pattern between $A\beta_{42}$ and Medin, as well as their structural characteristics at the atomic level, providing useful insights into the microscopic mechanism of $A\beta_{42}$ – Medin co-aggregation and the pathological mechanism of cross-correlation between different diseases.

2. Model and method

2.1 Simulation system: A$\boldsymbol{\beta}_{42}$/Medin homotrimer and A$\boldsymbol{\beta}_{42}$ – Medin heterotrimer

As a first step to understand the microscopic mechanism of the co-aggregation of $A\beta_{42}$ and Medin, we performed extensive all-atom REMD simulations to investigate the structural characteristics and physical interaction details of $A\beta_{42}$ and Medin co-aggregate at the atomic level. We built three simulation systems: $A\beta_{42}$ homotrimer (labeled A-A^{trimer}), Medin homotrimer (M-M^{trimer}) and $A\beta_{42}$ -Medin heterotrimer (A-M^{trimer}). The $A\beta_{42}$ and Medin proteins consist of 42 and 50 amino acid residues, respectively, and their sequences are: 1) $A\beta_{42}$: NH_3^+-^{1}DAEFRHDSGYEVHHQKLVFFAEDVGSNKGAIIGLMVGGVVIA^{42}-COO^-; 2) Medin: NH_3^+ -^{1}RLDKQGNFNAWVAGSYGNDQWLQVDLGSSKEVTGIITQGARNFGSVQ FVA^{50}-COO^-. To mimic the neutral pH condition in experiments, Lys (Lys^+), Arg (Arg^+), Asp (Asp^-), Glu (Glu^-) and N-terminus/C-terminus (NH_3^+, COO^-) of both peptides were all charged. A single $A\beta_{42}$ chain were taken from the fibril structure (PDB ID: 5OQV)[45] resolved

by cryo-electron microscopy to use as the $A\beta_{42}$ monomer and the Medin monomer was predicted by AlphaFold[46] online server. Then high-temperature MD simulations (at 500 K) of $A\beta_{42}$ and Medin monomers were performed to yield a series of monomer conformations with high structural diversity (shown in Figure S1 and Figure S2 of the Supplementary Material (online)). In order to avoid the influence of the initial structures of peptides on the simulation results and traverse the monomer conformation space as much as possible, we randomly selected 36 monomer conformations of $A\beta_{42}$ and Medin from their high-temperature conformation ensembles (as shown in Figure S1 (B) and Figure S2 (B) of the Supplementary Material (online)), ensuring that these conformations have a rich degree of collapse (R_g covers the whole range, including R_g large, medium and small conformations), and are dominated by disordered secondary structures. The time points corresponding to all the selected monomer conformations are listed in Supplementary Material Table S1 and Table S2 (online). Then, the gmx insert-molecules program and VMD software[47] were used to construct 12 $A\beta_{42}$ trimers and Medin trimers by placing monomers in different orientations (as shown in Figure S3 (a) and Figure S3 (B) of the supplementary material (online)). 12 $A\beta_{42}$-Medin heterotrimers ($A\beta_{42}$: Medin = 2:1, as shown in Figure S3 (C) of the Supplementary Material (online)) were built by replacing an Aβ in the 12 $A\beta_{42}$ trimers with Medin. In all trimers, the minimum monomer-to-monomer distance is greater than 0.6 nm, thus excluding initial artificial contact between the peptide chains. We used these $A\beta_{42}$, Medin, and $A\beta_{42}$-Medin trimer structures (12 for each) as the initial conformations for REMD simulations.

2.2 Simulation method

In this study, MD and REMD simulations were performed using GROMACS 2020.3 software package[48] combined with Amber99SB-ILDN force field[49,50] and TIP3P water model. Force field development aims to reproduce the properties of folded proteins consistent with experiments by optimizing force field parameters[51]. Traditional force fields such as Amber99SB-ILDN and CHARMM27 are widely used in MD/REMD simulations of amyloid proteins and their fragments, which can well describe the conformation and interaction of peptides, and the chemical shifts calculated from the simulation data are in good agreement with the experimental results of nuclear magnetic resonance (NMR)[41,42,52]. Nevertheless, early all-atom force fields tend to underestimate the radius of gyration (Rg) of proteins and overestimate the fraction of ordered secondary structures[53]. In order to alleviate the problem of over-compact conformation of disordered proteins, researchers have developed a series of new force fields and optimized water models by strengthening protein-water interactions and maintaining water-water and protein-protein interactions, such as Amber03ws[54], CHARMM36m[55] and TIP4P-D[56]. Interestingly, Zerze et al.[57] showed that the ability of the improved force field to assess protein compactness was independent of the accuracy of the propensity prediction of local secondary structures, indicating that the existing force field still

needs further improvement.

In all simulations, $A\beta_{42}$/Medin monomers and $A\beta_{42}$/Medin/$A\beta_{42}$ -Medin trimers were placed in the center of the box ($A\beta_{42}$ monomer: 8.25 nm × 8.25 nm × 8.25 nm, Medin monomer: 8.35 nm × 8.35 nm × 8.35 nm, trimer: 7.6 nm × 7.6 nm × 7.6 nm) with no interaction between the peptides and the mirror image. The box was filled with TIP3P water molecules, and Na^+ and Cl^- ions were added to neutralize the system and maintain a physiological salt concentration (0. 15 mol/L).

In high-temperature MD simulations, electrostatic interactions were treated with the Particle Mesh Ewald method (PME)[58] with a real space cutoff of 1.2 nm, and the van der Waals interactions were calculated using a cutoff of 1.2 nm. After energy optimization and equilibration, the initial velocities of the system were assigned according to the Maxwell-Boltzman velocity distribution.

The protein and non-protein groups were separately coupled to an external heat bath at 500 K with a coupling constant of 0.1 ps using a velocity rescaling method[59]. The pressure was kept at 1 bar using the Parrinello–Rahman method [60] with a coupling time constant of 1.0 ps. The high temperature MD simulation time was 13 ns for $A\beta_{42}$ monomer and 80 ns for Medin monomer.In REMD simulations, *N* replicas of the same system are simulated in parallel using MD simulations at different temperatures. Swapping between adjacent replicas is periodically attempted with a probability given by the Metropolis criterion. This method generates a generalized ensemble of the simulated system[33]. The conformations of peptides at low temperature have a certain probability to exchange to high temperature in REMD simulations, which accelerates the conformational transition of peptides, thus effectively avoiding the situation of peptide conformations trapping in the local potential well at low temperature. In our REMD simulations, A-A^{trimer}, M-M^{trimer} and A-M^{trimer} systems each contain 48 replicas, temperatures exponentially distributed from 308.18 K to 404.32 K (see Table S3 — Table S5 (online) for the temperature list). The REMD simulations were performed under the NPT ensemble with 500 ns simulation time per replica. Replica exchange was attempted every 2 ps and the average exchange rate of the three systems is larger than 20%. Periodic boundary conditions were applied in all simulations All-bond lengths were constrained using the SETTLE method [61] for water molecules and LINCS algorithm[62] for proteins, allowing an integration time step of 2 fs. Electrostatic interactions were treated using the PME method[58] with a real space cutoff of 1.2 nm. The van der Waals interactions were calculated using a cutoff of 1.2 nm. Protein and non-protein (water and ions) groups were separately coupled to an external heat bath with a coupling constant of 0.1 ps using the V-rescale method[59]. The pressure was kept at 1 bar using the Parrinello–Rahman method[60] with a coupling time constant of 1.0 ps.

2.3 Analytical method

All calculations and analyses were performed using our in-house developed codes and tools implemented in GROMACS software. Peptide secondary structure was identified by DSSP (define secondary structure of protein) program[63]. Cluster analysis was performed using the Daura method[64], and the corresponding cutoff of C_α-root mean square deviation (C_α-RMSD) was set to 0.30 nm. The interaction between peptides or amino acids is estimated by the contact probability. The criterion for contact is that the minimum carbon-carbon distance between residues is less than 0.54 nm, or the minimum distance between other non-hydrogen atoms is less than 0.46 nm[3, 14, 65, 66]. When the distance between N atom and O atom is less than 0.35 nm and the N — H ···O angle is greater than 150 °, H-bond is considered to be formed. The number of strands involved in the formation of a β-sheet is defined as the β-sheet size, and the number of residues continuously forming a β-strand is defined as the β-sheet length. Trajectory visualization and peptide structure representation were performed using VMD[47] and PyMOL[67,68] softwares.

3. Simulation results and discussion

Prior to data analysis, we checked the convergence of REMD simulations by calculating the time evolution of replica number at 310 K and comparing several quantities within two different time intervals (see Supplementary Material Figure S4 — Figure S6 (online)). The results show that at 310 K, all replicas in three systems can uniformly traverse the conformational ensembles of both $A\beta_{42}$ and Medin in the time range from 0 to 500 ns, and the simulation data from the two time periods (300-400 ns and 400-500 ns) coincide well in terms of the probability density function (PDF) of total hydrogen bond (H-bond) and contact number of peptides and

the probability of total hydrogen bond (H-bond) number, Rg and contact number of peptide trimers and the probability of each type of secondary structure, demonstrating that REMD simulations are nicely converged after 300 ns. Thus, all the results presented below are based on simulation data generated in the last 200 ns trajectories.

3.1 The $A\boldsymbol{\beta}_{42}$ has a higher affinity for Medin and co-aggregation alters the way the $A\boldsymbol{\beta}_{42}$ interacts with Medin

Firstly, the physical interactions in $A\beta_{42}$, Medin and $A\beta_{42}$/Medin trimer systems and the affinity (Fig. 1) between $A\beta_{42}$ and Medin were examined. According to the PDF of the number of contacts and hydrogen bonds of the peptide trimer (Fig. 1(a),Fig. 1(b)), we found that the interaction of Medin trimer was the strongest, followed by $A\beta_{42}$-Medin co-aggregation system, and the interaction of $A\beta_{42}$ trimer was the weakest. Meanwhile, the ability of $A\beta_{42}$-Medin to form hydrogen bonds with $A\beta_{42}$ trimers is weaker than that of Medin trimers. In the $A\beta_{42}$-Medin heterotrimer, there exists both the interactions between $A\beta_{42}$ and $A\beta_{42}$ and between Medin and Medin, and the binding between $A\beta_{42}$ and Medin is significantly

higher than that of $A\beta_{42}$ itself (Fig. 1(c),Fig. 1(d), dark blue vs. green). In addition, the $A\beta_{42}$-$A\beta_{42}$ interaction was lower in heterotrimers than in homotrimers (Fig. 1(c),Fig. 1(d), dark blue vs. light blue). These results suggest that the affinity between $A\beta_{42}$ and Medin is higher when $A\beta_{42}$ and Medin co-aggregate, and $A\beta_{42}$ prefers to interact with Medin rather than self-aggregate.

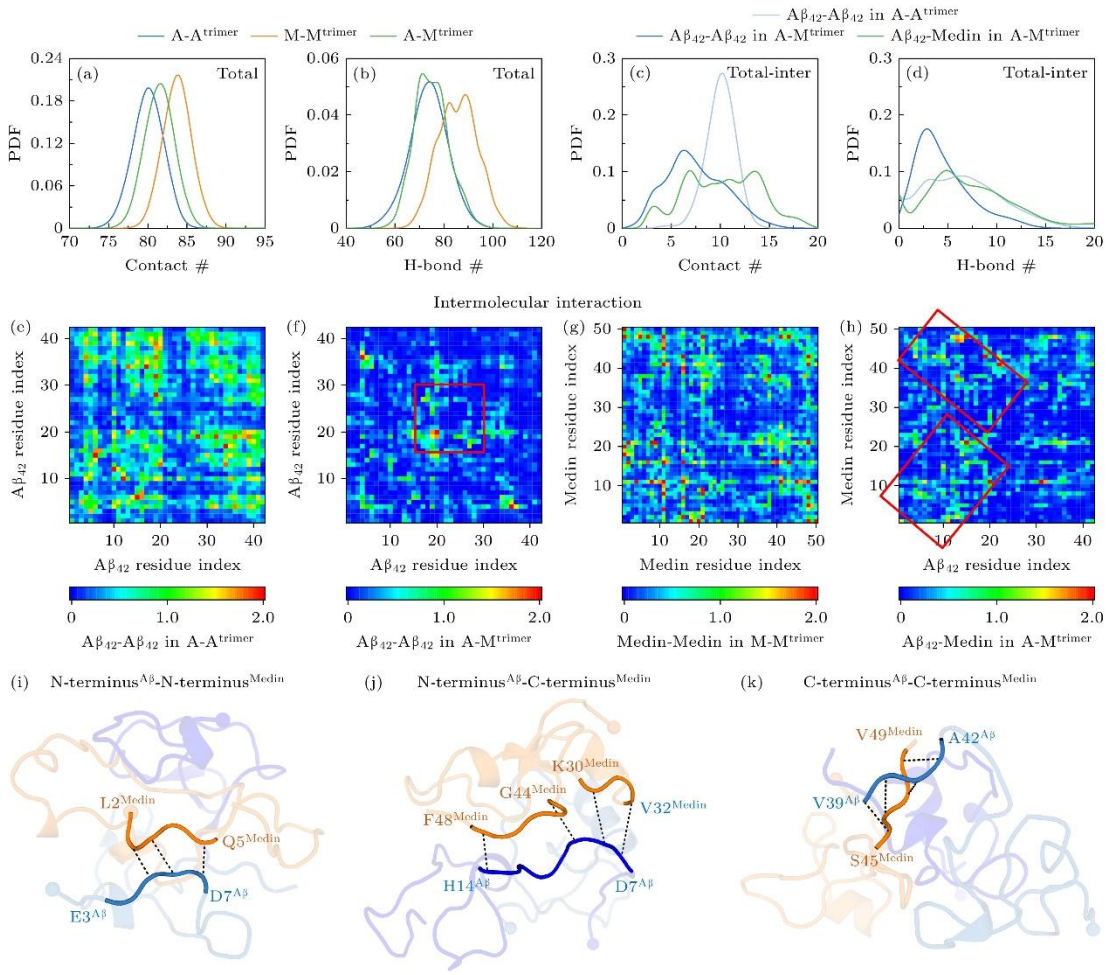

Figure 1. Analysis of interactions in $A\beta_{42}$/Medin homotrimers and $A\beta_{42}$-Medin heterotrimer: (a), (b) Probability density function (PDF) of (a) contact number and (b) hydrogen-bond (H-bond) number of peptides in three systems; (c), (d) PDF of (c) contact number and (d) H-bond number between $A\beta_{42}$ and $A\beta_{42}$ as well as between $A\beta_{42}$ and Medin in A-A^{trimer} and A-M^{trimer} systems; (e)–(h) 2D residue-residue contact maps of intermolecular interactions for (e) $A\beta_{42}$-$A\beta_{42}$ in A-A^{trimer}, (f) $A\beta_{42}$-$A\beta_{42}$ in A-M^{trimer}, (g) Medin-Medin in M-M^{trimer} and (h) $A\beta_{42}$-Medin in A-M^{trimer}; (i)–(k) representative snapshots illustrate the binding regions between $A\beta_{42}$ and Medin in A-M^{trimer} system.

In order to further explore the interaction mode and binding "hot spot" region between $A\beta_{42}$ and Medin during self-aggregation and co-aggregation, we calculated the residue-residue contact number map (Fig. 1(e) —(h)) between peptide molecules. In the

homotrimer, the number of residue contacts between $A\beta_{42}$ molecules is large, and the residue binding sites are concentrated between N-N terminus, N-C terminus and C-C terminus of $A\beta_{42}$, in which the hydrophobic contacts between Y10-V12, H6-Q15, F19-K28, F19-I32 and L34-L17 residue pairs are dominant (Fig. 1(e)). The representative structural snapshot in Figure S7 (a) (online) of the Supplementary Material shows the contact interaction of heavy atoms between F19-K28 and Y10-V12 residue pairs of $A\beta_{42}$. In contrast, in $A\beta_{42}$-Medin heterotrimer, the interaction strength and binding region between $A\beta_{42}$ molecules are significantly reduced. Interestingly, the interaction between the ^{16}KLVFFA^{21} region in the middle of the $A\beta_{42}$ peptide is instead enhanced (Fig. 1(f), see Supplementary Material Figure S7 (b) for contact details between L17-F20 and F20-F20 (online)).^{17}LVFFA^{21} has been proved to be the hydrophobic core region of $A\beta_{42}$, and efficient hydrophobic core stacking is essential for Aβ aggregation[39,69]. Our results indicate that the presence of Medin significantly changes the interaction mode between $A\beta_{42}$ molecules, resulting in that $A\beta_{42}$ only maintains the contact between hydrophobic cores but exhibits a higher degree of freedom in other regions, resulting in that $A\beta_{42}$ has the possibility of binding to Medin on the premise of ensuring its own aggregation ability. For the Medin homotrimer, the binding of Medin molecules is widely and uniformly distributed (except for the low number of contacts between D25-A40 and R1-S15), especially the contacts between hydrophobic and aromatic residue pairs such as K4-W11, F8-W11, W11-Y16, Y16-Y16 and W21-F48 are very strong (Fig. 1(g)), indicating that Medin molecules form a compact aggregation core through strong hydrophobic and π-π stacking interactions between amino acid side chains. Figure S7 (c) (online) of the Supplementary Material shows the π-π stacking interaction between aromatic amino acids containing benzene rings (F8 - W11 and W21 - F48). Through the residue-residue contact number map and the analysis of the binding sites between $A\beta_{42}$/Medin and each other (that is, the total number of contacts between Medin and each residue in $A\beta_{42}$ and the total number of contacts between $A\beta_{42}$ and each residue in Medin), we found that the binding sites between $A\beta_{42}$ and Medin were also abundant, basically throughout the whole peptide chain, in which the N-terminal of $A\beta_{42}$ was connected with the N-terminal of Medin, and the N-terminus of $A\beta_{42}$

and the C-terminus of Medin, as well as the C-terminus of $A\beta_{42}$ and the C-terminus of Medin are relatively strong. This indicates that the N-terminus of $A\beta_{42}$ and the C-terminus of Medin play an important role in the cross-interaction between $A\beta_{42}$ and Medin (Figure 1(h), Supplementary Material Fig S8(a), Fig S8(b) (online). Structural snapshots in Fig. 1(i) —(k) highlight the binding of different regions between $A\beta_{42}$ and Medin, which are $N^{A\beta}$ — N^{Medin}, $N^{A\beta}$ — C^{Medin}, and $C^{A\beta}$ — C^{Medin}. The binding sites between $A\beta_{42}$/Medin and each other through hydrogen bonding and hydrophobic interactions were further analyzed, that is, the number of hydrogen bonds and hydrophobic contacts between Medin and each residue in $A\beta_{42}$, and the number of hydrogen bonds and hydrophilic contacts between

$A\beta_{42}$ and each residue in Medin (as shown in Figure S8 (c)- (f) of the Supplementary Material (online)). As can be seen from Figure S8 (c)- (f) (online) of the Supplementary Material, the hydrogen bonding and hydrophobic binding sites of Medin on $A\beta_{42}$ tend to be concentrated on the N-terminal of $A\beta_{42}$, while those of $A\beta_{42}$ on Medin are distributed in the N-terminal and C-terminal regions of Medin, which reconfirms the key role of the N-terminal of $A\beta_{42}$ and the C-terminal of Medin. In particular, $Q15^{A\beta}$-$W21^{Medin}$, $Q15^{A\beta}$-$F48^{Medin}$, $F19^{A\beta}$-$F43^{Medin}$, $F20^{A\beta}$-$W11^{Medin}$, $E22^{A\beta}$-$R41^{Medin}$ and $I31^{A\beta}$-$W11^{Medin}$ are the residue pairs with strong binding between $A\beta_{42}$ and Medin (see Figure S7 (d) (online) of Supplementary Material for the binding between Fig. 1(h), F19-F43 and I31-W11). Medin forms obvious hydrogen bonds and hydrophobic interactions with A2/F4/H6/E11/H14/Q15 and F4/Y10/H13/F19/F20 of $A\beta_{42}$, respectively, while the number of hydrogen bonds and hydrophobic contacts between $A\beta_{42}$ and W11/E31/I35/I36/G39/R41 and F8/W11/Y16/W21/F43/F48 of Medin is higher (Supplementary Material Figure S8 (c) — (f) (online)). These results indicate that the binding between $A\beta_{42}$ and Medin is dependent on hydrogen bonding, hydrophobic and π-π stacking interactions.

More importantly, we found that $F19^{A\beta}$ and $W11^{Medin}$/$F48^{Medin}$ also play an important role in $A\beta_{42}$ and Medin homotrimer, indicating that $A\beta_{42}$ and Medin have the same molecular recognition sites or regions in both self-aggregation and co-aggregation. Finally, we analyzed the intramolecular interactions of the peptides in three systems. Through the intra-chain residue-residue contact number map of $A\beta_{42}$ and Medin in different systems (see Supplementary Material Figure S9 (online)), we found that the intra-chain interaction of $A\beta_{42}$ in heterotrimer showed an increase in the contact number of C-terminus and a decrease in the contact number of N-terminus compared with homotrimer systems (see Supplementary Material Figure S9 (a)- (c) (online)). Similarly, Medin peptides in heterotrimer system exhibit intrachain residue-residue interactions that are different from those in homotrimer systems (see Supplementary Material, Figure S9 (d)- (f) (online)). These results suggest that the co-aggregation of $A\beta_{42}$ and Medin changes the interaction mode of $A\beta_{42}$ and Medin.

3.2 Co-aggregation alters conformational characteristics of $A\boldsymbol{\beta}_{42}$ and Medin

In order to explore the effect of co-aggregation on the conformational space of peptide trimers, we chose the interchain contact number (inter-contact #) and the Rg of trimer as two reaction coordinates, and constructed the two-dimensional free energy landscapes (FELs) for the three simulation systems. As shown in Fig. 2(a), in the A-A^{trimer} system, the $A\beta_{42}$ homotrimer presents only one large minimum-energy basin, while in the M-M^{trimer} and A-M^{trimer} systems, the Medin homotrimer and $A\boldsymbol{\beta}_{42}$ – Medin heterotrimer present multiple dispersed minimum-energy basins, indicating that the conformational diversity of homotrimers formed by $A\beta_{42}$ and Medin is different (the former is lower, while the latter is higher), and that of heterotrimer is significantly increased. In addition, the free energy surface of the

$A\beta_{42}$ homotrimer is at 500≤inter-contact # ≤1750 and 1.35 nm≤R_g≤1. 65 nm range, while the free energy surface of the Medin homotrimer is located at 750≤inter-contact #≤2250 and 1.45 nm≤R_g≤1. 80 nm region, indicating that the interchain interaction of Medin trimer is stronger than that of $A\beta_{42}$ system and the trimer structure is relatively loose (Fig. 1(b),Fig. 1(c)). In contrast, the free energy surface of the heterotrimer is located at the center of the two self-aggregation systems (at 750 ≤inter-contact # ≤2000 and 1.40 nm≤R_g≤1.75 nm), implying that the interchain interaction of the co-assembly trimer is stronger than that of $A\beta_{42}$ trimer but weaker than that of Medin trimer as well as that the structure of heterotrimer is slightly looser than that of $A\beta_{42}$ trimer but relatively compact than Medin trimer (Fig. 2).

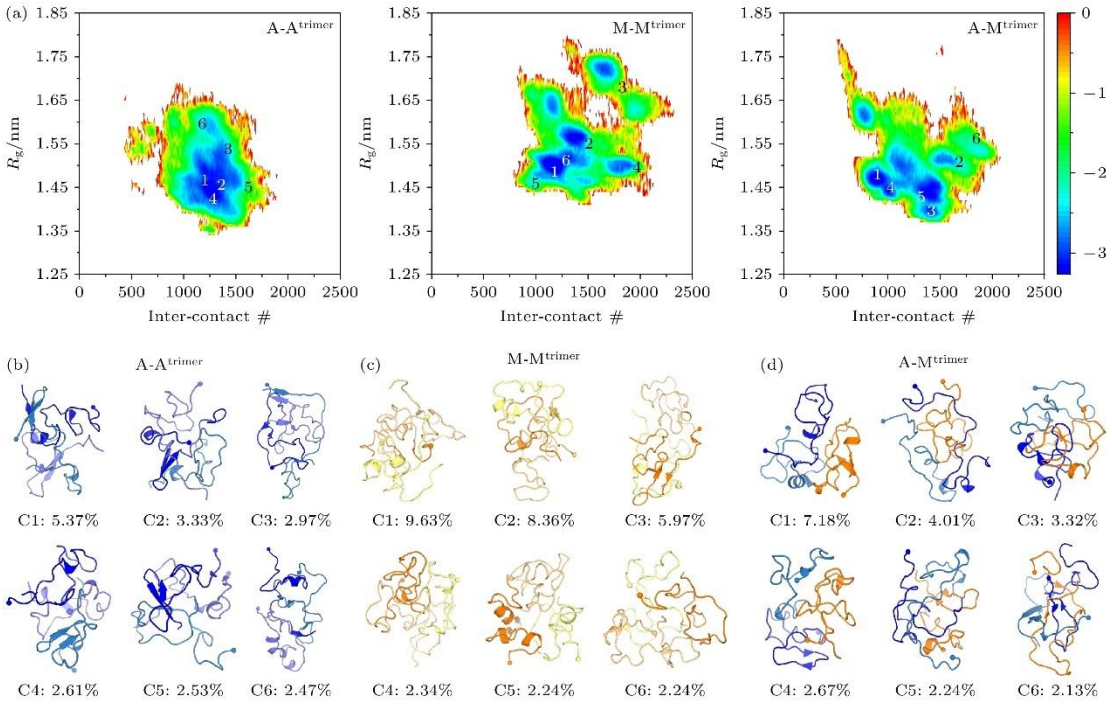

Figure 2. Analysis of conformational characteristics of $A\beta_{42}$/Medin homotrimers and $A\beta_{42}$-Medin heterotrimer: (a) FELs as a function of intermolecular contact number and trimeric R_g in A-A^{trimer} (left), M-M^{trimer} (middle) and A-M^{trimer} (right) systems; (b)–(d) representative conformations for the six most-populated clusters (C1–C6) along with their corresponding populations (marked below the corresponding representative conformations) of (b) $A\beta_{42}$ trimer, (c) Medin trimer and (d) $A\beta_{42}$-Medin trimer. The locations of those representative conformations are labeled on the FEL plots. $A\beta_{42}$ and Medin are shown in cartoon, with the N-terminal Cα atom of each chain represented by a sphere. $A\beta_{42}$ and Medin peptides are colored in blue and orange, respectively.

Moreover, cluster analysis is performed in three trimer systems and the representative conformations for the six most-populated clusters (C1 — C6) along with their corresponding populations were displayed in Fig. 2(b) —(d). It can be seen from the Fig. 2(a) that the

peptide conformations are mainly disordered (coil accounts for the highest proportion, followed by bend and turn structures) and contain a certain amount of ordered secondary structures (β and helix), while the overall conformations show different degrees of compactness ($M\text{-}M^{trimer}$<$A\text{-}M^{trimer}$<$A\text{-}A^{trimer}$). The top six clusters of $A\beta_{42}$ trimer are centered in the major minimum-energy basin of the free energy surface, while those of Medin and $A\beta_{42}$-Medin trimers are dispersed in multiple minimum-energy basins, providing evidence again for the different diversity of the self- and co-aggregated trimer conformations.

The aggregation of soluble monomers to β-sheet-rich fibrils is a marker of amyloidosis. In order to study the secondary structure of Aβ and Medin in self-aggregation and co-aggregation, we analyzed the propensity of each type secondary structure and the length/size of β-sheet structures of $A\beta_{42}$, Medin and $A\beta_{42}$ - Medin trimers (Fig. 3). In $A\beta_{42}$ trimer, the probability of β structure is 16.3%, which is higher than that of the other two trimers and higher than that of the helix structure formed by $A\beta_{42}$ (10.0%), indicating that at the trimer level, the ordered structure in $A\beta_{42}$ is dominated by β, and the ability of $A\beta_{42}$ self-aggregation to form β structure is stronger than that of Medin self-aggregation and $A\beta_{42}$-Medin co-aggregation. In Medin trimer, the proportion of β structure is 9.6%, which is the lowest among the three trimers, while the propensity of helix structure (10.7%) is slightly higher than that of β structure. Differently, in $A\beta_{42}$-Medin trimer, the β fraction (13.1%) of heterotrimer caused by co-aggregation is lower than that of $A\beta_{42}$ trimer but higher than that of Medin trimer, while the helix fraction (10.6%) is close to that of Medin trimer and slightly higher than that of $A\beta_{42}$ trimer. Furthermore, we calculated the probabilities of helix and β structures formed by $A\beta_{42}$ and Medin peptides in heterotrimer, respectively, and compared them with the corresponding homogeneous systems (Fig. 3(b),Fig. 3(c)). Our results show that $A\beta_{42}$ has a higher probability of forming helix in $A\beta_{42}$-Medin trimer than in homotrimer (Fig. 3(b), $A\beta_{42}^{*}$ vs. $A\beta_{42}$), while Medin has a significantly lower probability of forming helix than the homotrimer (Fig. 3(b), Medin * vs. Medin). In contrast, the probability of β structure of $A\beta_{42}$ in the co-aggregation system is significantly lower than that in the self-aggregation system (Fig. 3(c), $A\beta_{42}^{*}$ vs. $A\beta_{42}$), while the β probability of Medin in co-aggregated trimers is higher than that in self-aggregated trimers (Fig. 3(c), Medin * vs. Medin). These results suggest that the cross-interaction of the two peptides can promote Medin to form more β structure and reduce the appearance of helix structure, but induce $A\beta_{42}$ to form more helix structure and reduce β structure. Additionally, by analyzing the arrangement of β structures (interchain β-strands vs. intrachain β-strands), we found that the β structures in $A\beta_{42}$, Medin and $A\beta_{42}$-Medin trimers were mainly formed in the intrachain arrangement, and only a small amount of β structures exhibits the interchain arrangement (Fig. 3(d)). The probability of interchain β structures of $A\beta_{42}$ trimer is the highest, while the probabilities of intrachain β structures of Medin and $A\beta_{42}$-Medin trimers are much higher than that of $A\beta_{42}$. Interestingly, peptide co-aggregation induces the probability of interchain β structures being lower than that

in $A\beta_{42}$ trimer but slightly higher than that in Medin trimer.

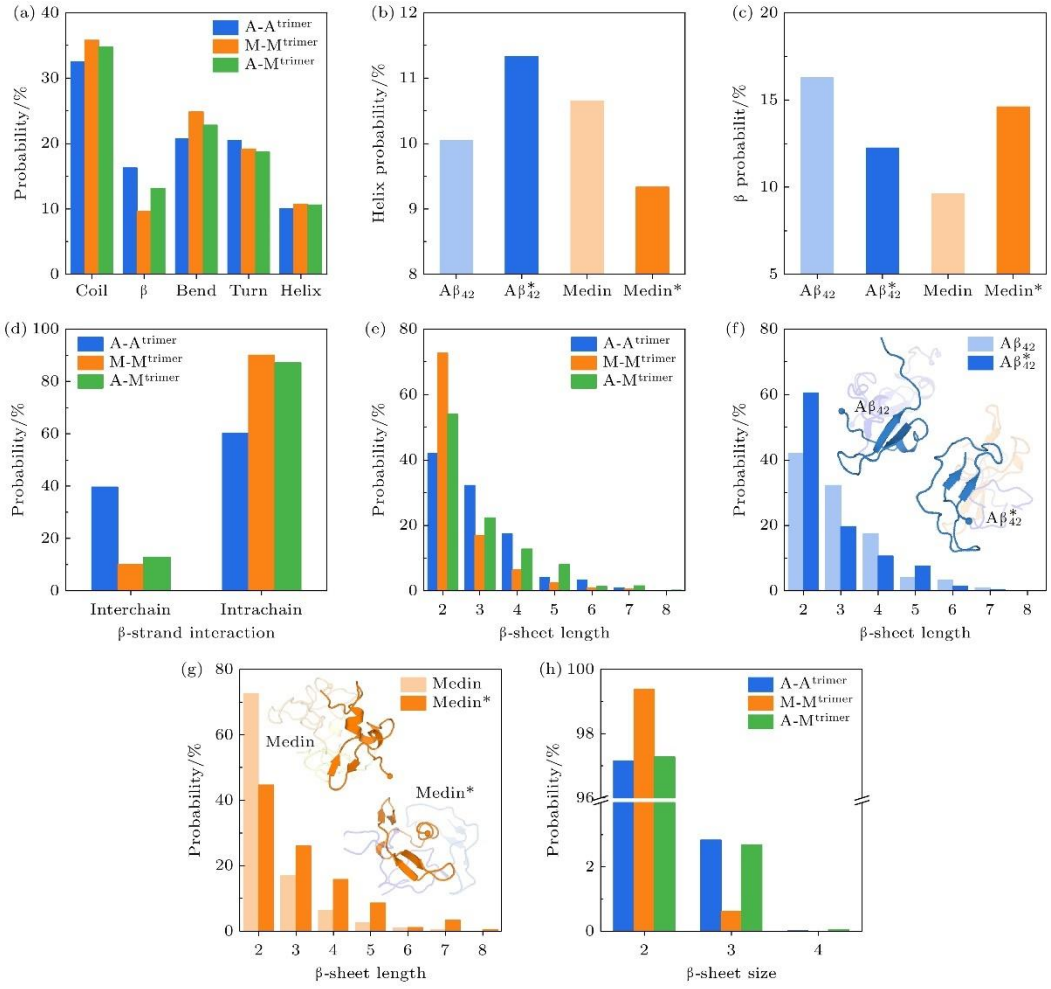

Figure 3. Analysis of secondary structures of $A\beta_{42}$/Medin homotrimers and $A\beta_{42}$-Medin heterotrimer: (a) Each secondary structure probability of $A\beta_{42}$ homotrimer, Medin homotrimer and $A\beta_{42}$-Medin heterotrimer; (b) helix probability of $A\beta_{42}$ and Medin in different systems: $A\beta_{42}$ in A-A^{trimer} system (light blue) vs. $A\beta_{42}$ in A-M^{trimer} system (*, blue) and Medin in M-M^{trimer} system (light orange) vs. Medin in A-M^{trimer} system (*, orange); (c) β probability of $A\beta_{42}$ and Medin in different systems; (d) probability of β arrangement with interchain and intrachain manners; (e) probability of β-sheet length in three systems; (f) probability of β-sheet length of $A\beta_{42}$ in A-A^{trimer} and A-M^{trimer} systems; (g) probability of β-sheet length of Medin in M-M^{trimer} and A-M^{trimer} systems; (h) probability of β-sheet size in three systems.

In order to further understand the influence of different peptide environments on the β structure, we calculated the length and size (Fig. 3(e) —(h)) of the β-sheet structure formed by $A\beta_{42}$ and Medin. The results show that in three systems, the β-sheet structures of different trimers mainly possess a length of 2-4, along with a low probability of forming a longer (5-7) β-sheet (Fig. 3(e)). Compared with the other two trimers, Medin homotrimer exhibits a significantly higher probability of forming β-sheets with a length of 2 and a lower probability

to form β-sheets with length of 3-5. In $A\beta_{42}$ - Medin system, the probability of β sheets with the length of 2 and 3-4 is higher and lower than that in homo-$A\beta_{42}$ system, respectively. It is worth noting that the co-aggregation system has a higher ability to form β-sheet structure with longer length of 5 and 7. In particular, for $A\beta_{42}$ peptide, the probability of forming β-sheets with the length of 2 and 5 is higher in heterotrimer than in homotrimer (Fig. 3(f), $A\beta_{42}^{*}$ vs. $A\beta_{42}$). The probability of Medin forming β-sheets with the length of 2 in heterotrimer is lower than that in homotrimer, but the probability of longer length (3-7) in heterotrimer is significantly higher than that in homotrimers (Fig. 3(g), Medin * vs. Medin). Representative structural snapshots in Fig. 3(f) and Fig. 3(g) show that $A\beta_{42}$ forms a longer β in self-aggregates, while Medin forms a longer β in co-aggregates. Moreover, the analysis of β-sheet size shows that all trimers can only form β-sheets with the size of 2 and 3. The corresponding probabilities in $A\beta_{42}$ and $A\beta_{42}$-Medin systems are very similar, but those in Medin system is relatively large and small, respectively (Fig. 3(h)).

To investigate the influence of $A\beta_{42}$ – Medin co-aggregation on the distribution of ordered secondary structures, we calculated the probabilities of β and helix structures of each amino acid in $A\beta_{42}$ and Medin peptides (Fig. 4 and Supplementary Material Figure S10 (online)). Four regions (^{3}EFR^{5}, ^{17}LVFFA^{21}, ^{30}AII^{33} and ^{39}VVI^{41}) of $A\beta_{42}$ in homotrimer exhibit high propensity to form β structures, which are almost evenly distributed in the N-terminal, middle and C-terminal domain of Aβ peptides (Fig. 4(a)). In heterotrimer system, the high β-prone regions of $A\beta_{42}$ basically remain unchanged with decreased probabilities, while the neighboring regions (^{6}HD^{7}, ^{13}HHQK^{16} and ^{34}LMV^{36}) display increased probabilities of β structures (Fig. 4(c)). The representative snapshots in Fig. 4(a) and Fig. 4(c) illustrate the β-sheet-rich regions of $A\beta_{42}$ in $A\beta_{42}$ and $A\beta_{42}$-Medin trimers. The overall β probabilities of residues in homo-Medin system are low and only multiple small regions possess relatively high β probability, such as ^{8}FNAW^{11}, ^{16}YG^{17}, ^{20}QWLQVD^{25}, ^{30}KEVTGIIT^{37}, ^{41}RNF^{43} and^{47}QFV^{49} (Fig. 4(b)). Differently, the residue-specific β probability of Medin in heterotrimer increased significantly and the high β propensity regions changed from uniform distribution to be concentrated in the middle and C-terminal domains (^{4}KQGN^{7}, ^{20}QWLQVDLGSS^{29}, ^{36}ITQ^{38}, ^{41}RN^{42} and ^{44}GSVQFV^{49}) (Fig. 4(d)). Compared with $A\beta_{42}$, the β-sheet-rich regions of Medin in both homotrimer and heterotrimer are more abundant and dispersed, and the β-sheet structures are relatively short (representative snapshots of Medin and $A\beta_{42}$-Medin trimers in Fig. 4(b) and Fig. 4(d)).

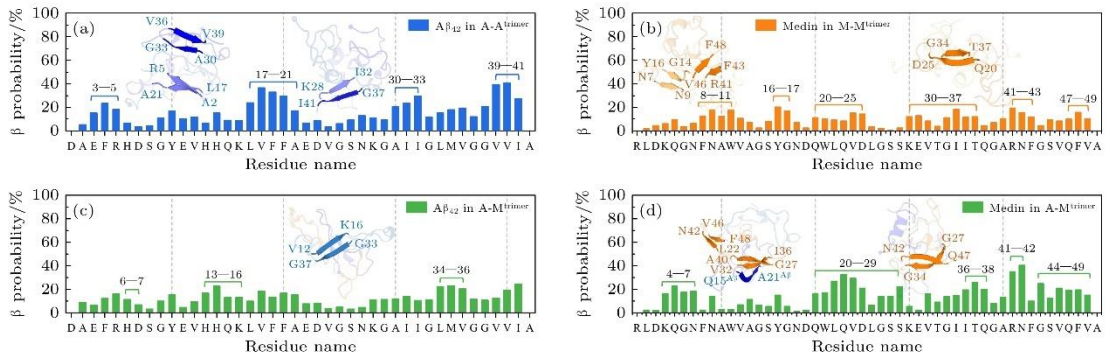

Figure 4. β-sheet probability and β-sheet formation regions of $A\beta_{42}$ and Medin in homotrimer and heterotrimer. Residue-based β probability distribution of $A\beta_{42}$ and Medin peptides respectively in (a) $A\beta_{42}$ homotrimer/(b) Medin homotrimer and (c), (d) $A\beta_{42}$-Medin heterotrimer. Representative β-sheet-rich conformations of $A\beta_{42}$, Medin and $A\beta_{42}$-Medin trimers are illustrated as insets in (a)–(d). $A\beta_{42}$ and Medin peptides are shown in cartoon with the β-sheet-rich regions highlighted in blue and orange, respectively.

Early experimental studies reported that three β-strand regions exist in Medin peptide and the ^{42}NFGSVQFV^{49} region in C-terminus is an important aggregation and amyloidosis motif of Medin[8].^{42}NFGSVQFV^{49} itself can rapidly aggregate to fibrils[11]. Reches and Gazit et al.[70] observed the formation and morphology of ^{42}NFGSVQFV^{49} fibrils by electron microscopy, and Madine et al.[71] utilized solid-state NMR and X-ray diffraction to identify the cross-β characteristics and atomic details of ^{42}NFGSVPFV^{49} fibrils. By combining Congo red staining, ThT fluorescence, transmission electron microscopy and other experimental methods, Westermark and co-workers[11] characterized the aggregation capability and fibrillar morphology of a series of synthetic Medin peptides (Medin constructs with different length), and determined that the 18-19 residues located at the end of Medin sequence were the key regions for Medin-Medin recognition and Medin aggregation. The TANGO algorithm based on statistical mechanics predicts that three regions in the Medin sequence, including^{43}FGSVQFV^{49}, have a high tendency for aggregation (the other two regions are ^{8}FNAWVAGSY^{16} and ^{32}VTGIIT^{37})[11]. ^{13}C-NMR experiment combined with ab initio protein modeling revealed that soluble Medin monomer possesses a stable core region (consisting of three β-strands) and a two β-strand region at the C-terminus. Moreover, MD simulations showed that the movement and conformational changes of C-terminal domain is essential for initiating the dimerization and subsequent aggregation of Medin[24]. By using solid state NMR experiments, Davies et al.[23] characterized the structure of Medin fibril and observed that Medin molecules contain at least two extended β-sheet regions, which form a β-hairpin structure induced by the D25-K30 salt bridge interaction. These results indicate that there are several β-sheet-rich regions in Medin, Specifically, ^{42}NFGSVQFV^{49} has a strong aggregation capacity and is considered as the core fragment for Medin fibrillization. Our simulation results are consistent with the β structural characteristics of Medin determined by various

experimental methods, and indicate that the C-terminal region of Medin (especially the ^{42}NFGSVQFV^{49} core fragment) would drive its co-aggregation with $A\beta_{42}$ by form a β-structure as a core site, thus playing a pivotal role in the co-aggregation process. It is worth notice that the presence of $A\beta_{42}$ promotes the formation of β structures in the C-terminal domain of Medin, suggesting that $A\beta_{42}$ - Medin co-aggregation may accelerate the overall aggregation of both peptides through this mechanism and affect the balance and interconversion between peptide oligomers and fibrils, leading to the regulation of the cytotoxicity of amyloid aggregates.

In contrast with the β structures, the high probability regions of helix structures formed by $A\beta_{42}$ and Medin in homo- or heterotrimers are relatively concentrated (see Supplementary Material Figure S10 (online)). The N-terminal ^{10}YEVHHQ^{15} and the C-terminal ^{32}IGLMV^{36} regions of $A\beta_{42}$ in homotrimer have high probabilities of forming helix (see Supplementary Material Figure S10 (a) (online)), while the helix probabilities of those two regions of $A\beta_{42}$ in heterotrimer are significantly decreased and increased, respectively (see Supplementary Material Figure S10 (c) and Figure S10 (e) (online)). In Medin trimer, regions with high helix propensities are relatively long and distributed in the whole peptide chain (^{6}GNFNAWVA^{13}, ^{19}DQWL^{22} and ^{29}KEVTGIIIQGARNFGS^{45}) (as shown in Supplementary Figure S10(b) (online)). Differently, in heterotrimer, the overall helix probability of Medin decreases, except for ^{19}DQWL^{22} and ^{33}GIII^{36} regions (as shown in Supplementary Figures S10(d) and S10(f) (online)).

4. Conclusion

By performing extensive all-atom REMD simulations, we investigated the conformational ensembles of $A\beta_{42}$ and Medin homotrimers, and the influence of co-aggregation on the physical interactions and structural properties of $A\beta_{42}$ and Medin. Our simulation results show that the affinity between $A\beta_{42}$ and Medin was higher than that of homopeptides ($A\beta_{42}$ - $A\beta_{42}$ and Medin-Medin), which provides the basis for the cross-interaction of the two peptides. $A\beta_{42}$ – Medin co-aggregation significantly changed the strength and pattern of intra- and intermolecular interactions between $A\beta_{42}$ and Medin. $A\beta_{42}$ - $A\beta_{42}$ interactions in homotrimer are the weakest and the binding sites are concentrated between N-N, N-C and C-C terminal domains, while the Medin - Medin interactions in homotrimer are the strongest and the binding sites disperse widely and evenly in the whole peptide chain.

Differently, in $A\beta_{42}$-Medin heterotrimer, $A\beta_{42}$ - $A\beta_{42}$ interactions decrease and only the binding between hydrophobic regions (^{16}KLVFFA^{21}) is retained, resulting in that $A\beta_{42}$ possesses the capability of binding with Medin on the premise of ensuring its own aggregation. $A\beta_{42}$ and Medin exhibit similar molecular recognition sites or regions in both self- aggregation and co-aggregation process. The binding sites between $A\beta_{42}$ and Medin are abundant, especially between N-terminus$^{A\beta}$ and N-terminus^{Medin}, N-terminus$^{A\beta}$ and

C-terminus^{Medin} and C-terminal$^{A\beta}$ and C-term^{Medin}, indicating that the N-terminus of $A\beta_{42}$ and the C-terminus of Medin play important roles in the cross-aggregation of $A\beta_{42}$ and Medin. The conformational diversities of $A\beta_{42}$ and Medin self-aggregates are different and that of $A\beta_{42}$-Medin trimers is increased induced by co-aggregation. The trimeric conformations of $A\beta_{42}$ and Medin peptides are mainly disordered, along with a relatively small proportion of ordered β and helix structures. $A\beta_{42}$-Medin co-aggregation leads to a decrease in the probability of high-β-propensity regions of $A\beta_{42}$, and induces the uniformly distributed high-β-propensity regions of Medin to relocate in the middle and C-terminal domains, implying that Medin would form β structures in C-terminus as a core motif to drive the co-aggregation with $A\beta_{42}$.

Our study elucidates the physical interactions and structural characteristics of $A\beta_{42}$ and Medin in different peptide environments (self-aggregation vs. co-aggregation) at the atomic level, providing useful insights into the molecular mechanism of $A\beta_{42}$ and Medin co-aggregation and the cross pathological mechanism of different diseases. According to our simulation results, compared with peptide self-aggregation, co-aggregation induces the formation of distinct β-sheet-rich regions on $A\beta_{42}$ and Medin. The core motifs with high β propensity and the intra-/intermolecular binding regions construct unique peptide-peptide biological interfaces. Therefore, future studies focus on the properties of those critical interfaces and their capability of driving the subsequent fibrillation would shed light on the therapeutic method development of targeting the peptide-peptide interface and destroying the key interfacial interactions.

References

[1] Giordano X, Fernandez M C 2023 Alzheimers Dementia. 19 e075955

[2] Scheltens P, De Strooper B, Kivipelto M, Holstege H, Chételat G, Teunissen C E, Cummings J, van der Flier W M 2021 Lancet 397 1577

[3] Li X, Yang Z, Chen Y, Zhang S, Wei G, Zhang L 2023 J. Phys. Chem. B 127 4050

[4] Ball K A, Phillips A H, Wemmer D E, Head-Gordon T 2013 Biophys. J. 104 2714

[5] Li X, Zhang Y, Wang Y, Zhang S, Zhang L 2024 J. Phys. Chem. B 128 1843

[6] Nunan J, Small D H 2000 FEBS Lett. 483 6

[7] Huang Y, Potter R, Sigurdson W, Santacruz A, Shih S, Ju Y E, Kasten T, Morris J C, Mintun M, Duntley S, Bateman R J 2012 Arch. Neurol. 69 51

[8] Häggqvist B, Näslund J, Sletten K, Westermark G T, Mucchiano G, Tjernberg L O,

Nordstedt C, Engström U, Westermark P 1999 Proc. Natl. Acad. Sci. U. S. A. 96 8669

[9] Karamanova N, Truran S, Serrano G E, Beach T G, Madine J, Weissig V, Davies H A, Veldhuizen J, Nikkhah M, Hansen M, Zhang W, D'Souza K, Franco D A, Migrino R Q 2020 J. Am. Heart Assoc. 9 e014810

[10] Madine J, Davies H A, Migrino R Q, Ruotsalainen S E, Wagner J, Neher J J 2023 Nat. Aging 3 1039

[11] Larsson A, Söderberg L, Westermark G T, Sletten K, Engström U, Tjernberg L O, Näslund J, Westermark P 2007 Biochem. Biophys. Res. Commun. 361 822

[12] Eisenberg D, Jucker M 2012 Cell 148 1188

[13] Iadanza M G, Jackson M P, Hewitt E W, Ranson N A, Radford S E 2018 Nat. Rev. Mol. Cell Biol. 19 755

[14] Ren B, Zhang Y, Zhang M, Liu Y, Zhang D, Gong X, Feng Z, Tang J, Chang Y, Zheng J 2019 J. Mater. Chem. B 7 7267

[15] Zhang Y, Tang Y, Zhang D, Liu Y, He J, Chang Y, Zheng J 2021 Chin. J. Chem. Eng. 30 225

[16] Migrino R Q, Karamanova N, Truran S, Serrano G E, Davies H A, Madine J, Beach T G 2020 Alzheimers Dementia 12 e12072

[17] Tayler H, Miners J S, Güzel Ö, MacLachlan R, Love S 2021 Brain Pathol. 31 e12935

[18] Benson M D, Buxbaum J N, Eisenberg D S, Merlini G, Saraiva M J M, Sekijima Y, Sipe J D, Westermark P 2020 Amyloid 27 217

[19] Jackson R J, Rudinskiy N, Herrmann A G, Croft S, Kim J M, Petrova V, Ramos-Rodriguez J J, Pitstick R, Wegmann S, Garcia-Alloza M, Carlson G A, Hyman B T, Spires-Jones T L 2016 Eur. J. Neurosci. 44 3056

[20] Wagner J, Degenhardt K, Veit M, Louros N, Konstantoulea K, Skodras A, Wild K, Liu P, Obermüller U, Bansal V, Dalmia A, Häsler L M, Lambert M, De Vleeschouwer M, Davies H A, Madine J, Kronenberg-Versteeg D, Feederle R, Del Turco D, Nilsson K P R, Lashley T, Deller T, Gearing M, Walker L C, Heutink P, Rousseau F, Schymkowitz J, Jucker M, Neher J J 2022 Nature 612 123

[21] Huang F, Fan X, Wang Y, Zou Y, Lian J, Wang C, Ding F, Sun Y 2024 Brief. Bioinform. 25 bbad526

[22] Howitz W J, Wierzbicki M, Cabanela R W, Saliba C, Motavalli A, Tran N, Nowick J S 2020 J. Am. Chem. Soc. 142 15870

[23] Davies H A, Madine J, Middleton D A 2015 J. Biol. Chem. 290 7791

[24] Davies H A, Rigden D J, Phelan M M, Madine J 2017 Sci. Rep. 7 45224

[25] Huang F, Yan J, Zhang X, Xu H, Lian J, Yang X, Wang C, Ding F, Sun Y 2024 Colloids Surf. , B 244 114192

[26] Huang F, Fan X, Wang Y, Wang C, Zou Y, Lian J, Ding F, Sun Y 2023 J. Chem. Inf. Model. 63 6376

[27] Xu C, Lin Z, Yang K, Yuan B 2020 Acta Phys. Sin. 69 108701

[28] Wang K, Xu C, Wu J F, Yang K, Yuan B 2021 Acta Phys. Sin. 70 178701

[29] Tan J P, Zhang W T, Xu C, Lu X M, Zhu W S, Yang K, Yuan B 2024 Acta Phys. Sin. 73 188702

[30] Tu W, Dong X, Ou L, Zhang X, Yuan B, Yang K 2023 Chem. Res. Chin. Univ. 39 829

[31] Lao Z, Tang Y, Dong X, Tan Y, Li X, Liu X, Li L, Guo C, Wei G 2024 Nanoscale 16 4025

[32] Liu X, Lao Z, Li X, Dong X, Wei G 2022 Phys. Chem. Chem. Phys. 24 16263

[33] Qi R, Wei G, Ma B, Nussinov R 2018 Methods Mol. Biol. 1777 101

[34] Sugita Y, Okamoto Y 1999 Chem. Phys. Lett. 314 141

[35] Miron R A, Fichthorn K A 2003 J. Chem. Phys. 119 6210

[36] K ästner J 2011 Wiley Interdiscip. Rev. Comput. Mol. Sci. 1 932

[37] Qi R, Luo Y, Wei G, Nussinov R, Ma B 2015 J. Phys. Chem. Lett. 6 3276

[38]Dong X, Bera S, Qiao Q, Tang Y, Lao Z, Luo Y, Gazit E, Wei G 2021 J. Phys. Chem. Lett. 12 2576

[39] Li X, Chen Y, Yang Z, Zhang S, Wei G, Zhang L 2024 Int. J. Biol. Macromol. 254 127841

[40] Tan Y, Chen Y, Liu X, Tang Y, Lao Z, Wei G 2023 Int. J. Biol. Macromol. 241 124659

[41] Lao Z, Dong X, Liu X, Li F, Chen Y, Tang Y, Wei G 2022 J. Chem. Inf. Model. 62 3227

[42] Dong X, Qi R, Qiao Q, Li X, Li F, Wan J, Zhang Q, Wei G 2021 Phys. Chem. Chem. Phys. 23 20406

[43] Mo Y, Brahmachari S, Lei J, Gilead S, Tang Y, Gazit E, Wei G 2018 ACS Chem. Neurosci. 9 2741

[44] Guo C, Côté S, Mousseau N, Wei G 2015 J. Phys. Chem. B 119 3366

[45] Gremer L, Schölzel D, Schenk C, Reinartz E, Labahn J, Ravelli R B G, Tusche M, Lopez-Iglesias C, Hoyer W, Heise H, Willbold D, Schröder G F 2017 Science 358 116

[46]Jumper J, Evans R, Pritzel A, Green T, Figurnov M, Ronneberger O, Tunyasuvunakool K, Bates R, Žídek A, Potapenko A, Bridgland A, Meyer C, Kohl S A A, Ballard A J, Cowie A, Romera-Paredes B, Nikolov S, Jain R, Adler J, Back T, Petersen S, Reiman D, Clancy E, Zielinski M, Steinegger M, Pacholska M, Berghammer T, Bodenstein S, Silver D, Vinyals O, Senior A W, Kavukcuoglu K, Kohli P, Hassabis D 2021 Nature 596 583

[47] Humphrey W, Dalke A, Schulten K 1996 J. Mol. Graphics 14 33

[48] Abraham M J, Murtola T, Schulz R, Páll S, Smith J C, Hess B, Lindahl E 2015 SoftwareX 1–2 19

[49] Lindorff-Larsen K, Piana S, Palmo K, Maragakis P, Klepeis J L, Dror R O, Shaw D E 2010 Proteins 78 1950

[50] Chen Y, Li X, Zhan C, Lao Z, Li F, Dong X, Wei G 2021 ACS Chem. Neurosci. 12 4007

[51] Lopes P E, Guvench O, MacKerell Jr. A D 2015 Methods Mol. Biol. 1215 47

[52] Tan Y, Chen Y, Pan T, Tang Y, Liu X, Yu Y, Wei G 2025 J. Chem. Inf. Model. 65 4643

[53] Wang W 2021 Phys. Chem. Chem. Phys. 23 777

[54] Best R B, Zheng W, Mittal J 2014 J. Chem. Theory Comput. 10 5113

[55] Huang J, Rauscher S, Nawrocki G, Ran T, Feig M, de Groot B L, Grubmüller H, MacKerell A D, Jr. 2017 Nat. Methods 14 71

[56] Piana S, Donchev A G, Robustelli P, Shaw D E 2015 J. Phys. Chem. B 119 5113

[57] Zerze G H, Zheng W, Best R B, Mittal J 2019 J. Phys. Chem. Lett. 10 2227

[58] Parrinello M, Rahman A 1981 J. Appl. Phys. 52 7182

[59] Bussi G, Donadio D, Parrinello M 2007 J. Chem. Phys. 126 014101

[60] Li M, Johnson W L, Goddard W A 1992 MRS Online Proc. Lib. 291 285

[61] Miyamoto S, Kollman P A 1992 J. Comput. Chem. 13 952

[62] Hess B 2008 J. Chem. Theory Comput. 4 116

[63] Kabsch W, Sander C 1983 Biopolymers 22 2577

[64] Daura X, Gademann K, Jaun B, Seebach D, van Gunsteren W F, Mark A E 1999 Angew.

Chem. Int. Ed. 38 236

[65] Zhang Y, Liu Y, Zhao W, Sun Y 2021 Int. J. Biol. Macromol. 193 1

[66] Li X, Lao Z, Zou Y, Dong X, Li L, Wei G 2021 J. Phys. Chem. B 125 2050

[67] Delano W L http://pymol.org [2025-5-10]

[68] Rigsby R E, Parker A B 2016 Biochem. Mol. Biol. Educ. 44 433

[69] Okumura H, Itoh S G 2022 Molecules 27 2483

[70] Reches M, Gazit E 2004 Amyloid 11 81

[71] Madine J, Copland A, Serpell L C, Middleton D A 2009 Biochemistry 48 3089